Reactive Power Compensation Capabilities of V2G-Enabled Electric Vehicles

Giuseppe Buja, *Life Fellow, IEEE*, Manuele Bertoluzzo, and Christian Fontana, *Member, IEEE*

***Abstract*—Vehicle-to-grid (V2G) paradigm is a way of executing services in favor of the grid by electric vehicles (EVs) with bidirectional battery chargers (BBC). The V2G service that has attracted the major interest is the exchange of active power for load leveling purposes. Less attention has received the so-called ancillary V2G services, such as the reactive power compensation. This service is much attractive since it does not involve any exchange of active power and, therefore, leaves the EV batteries charged and does not expose them to additional discharging–charging cycles. The purpose of this paper is to investigate the capabilities of V2G-enabled EVs in executing the reactive power compensation, whether done alone or simultaneously with either battery charging or battery power delivery to the grid. Two topologies of BBC are examined, namely the topologies with the dc side of the charger either directly connected to the battery or through a bidirectional dc–dc converter of buck type. This paper closes by reporting experimental results that corroborate the theoretical findings.**

***Index Terms*—Bidirectional battery chargers (BBCs), electric vehicles (EVs), reactive power compensation, vehicle to grid (V2G).**

Nomenclature

AR	Active rectifier.
BBC	Bidirectional battery charger.
BDDC	Bidirectional dc–dc converter.
CC/CV	Constant-current/constant-voltage battery-charging stage.
I_b	Battery current.
$I_{\rm CC}$	CC stage maximum battery-charging current.
$I_{b,M}$	Maximum battery-discharging current.
i_i	AR ac-side current.
I_R	Rated AR current.
P_b	Battery power.
P_R	Rated AR active power.
Q_R	Rated AR reactive power.
Q_m	Minimum reactive power.
V_b	Battery voltage.
$V_{b,m}$	Battery minimum (cut off) voltage.
$V_{b,M}$	Battery maximum voltage.
$V_{\rm dc}$	AR dc-side voltage.
v_i	AR ac-side line-to-line voltage.
v_g	Grid voltage.
V_R	Rated AR voltage.
V_u	AR ac-side line-to-line voltage upper limit.

Throughout this paper, lower-case letters denote variable quantities. Upper-case letters denote both the rms value of sinusoidal quantities and the amplitude of constant or slowly varying quantities. Upper-case letters with a bar as superscript denote phasor quantities.

Manuscript received August 5, 2016; revised November 3, 2016 and January 17, 2017; accepted January 20, 2017. Date of publication January 25, 2017; date of current version August 2, 2017. Recommended for publication by Associate Editor M. Ferdowsi.

The authors are with the Department of Industrial Engineering, University of Padova, via Gradenigo 6a, Padova, 35131, Italy (e-mail: giuseppe.buja@unipd.it; manuele.bertoluzzo@unipd.it; christian.fontana@studenti.unipd.it).

Color versions of one or more of the figures in this paper are available online at http://ieeexplore.ieee.org.

Digital Object Identifier 10.1109/TPEL.2017.2658686

I. Introduction

THE expected proliferation of electric vehicles (EVs) has led to look at them not only as a load for the grid but also as a resource, according to the vehicle-to-grid (V2G) paradigm [1]–[4]. To implement V2G, EVs must be equipped with bidirectional battery chargers (BBCs) [5], [6], and be integrated in distributed networks [7], [8], smart grids [9], or even dc grids [10]. A number of circuitry arrangements have been proposed for the power converters interfacing the grid with the battery of EVs [11]–[13]; in addition to the conventional active rectifiers (AR), matrix converters are examined in [14] and converters obtained by a reconfiguration of the EV traction inverter in [15]–[17]. Wireless battery chargers with V2G facility have been also studied, based on inductive [18], [19] or capacitive [20] coupling.

According to V2G, charging of the EV batteries from the grid is enabled when there is a plenty of electric energy production, while power delivery from the EV batteries to the grid is exploited when there is a plenty of electric energy demand (load leveling). Besides load leveling, there is an emerging interest in evaluating other services that EVs can do in favor of the grid, especially in the smart grid prospective [21], [22]. They are commonly termed ancillary V2G services. Some of them are peak shaving, spinning reserve, frequency stabilization, and reactive power compensation. Although all of them are beneficial for the grid, some concerns are turned to the services involving an exchange of active power [23]. Concerns are related to both the chance of having available EVs with a nonadequately charged battery at the time of their need and the shortened working life of the battery for the additional discharging–charging cycles. Opposite to this, the reactive power compensation does not involve any exchange of active power and, for this reason, it appears of great interest [24], also for applications such as railways [25].

The above-quoted papers on V2G are mainly focused on functioning of BBCs, arrangement and sizing of the power converters, and development of the control algorithms. This paper,

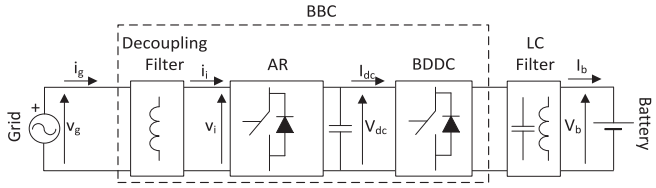

Fig. 1. General BBC block scheme.

instead, is focused on determining the capabilities of BBCs in accomplishing the reactive power compensation and demonstrates that they are dictated by the characteristics of the battery rather than by the arrangement and the control algorithm of the BBC itself. More specifically, this paper considers a BBC designed to charge the battery of a given EV and, consequently, sized according to the specifications of the battery of that EV. The capabilities of the resultant BBC in compensating for the reactive power are then evaluated in terms of the maximum amount of reactive power absorbed by BBC as a function of the actual battery state of charge and the BBC task, i.e., whether BBC is executing the reactive power compensation alone or simultaneously with either battery charging or battery power delivery. Two BBC topologies are considered, depending on whether or not the minimum level of the EV battery voltage is higher enough than the rectified grid voltage. In the first case, designated as topology #1, BBC is built up around an AR, while in the other case, designated as topology #2, BBC includes a bidirectional dc–dc converter (BDDC) of buck type in cascade to AR [26], [27].

This paper is organized as follows. Section II reviews the basic equations of BBC. Section III utilizes the current and voltage specifications of a battery to determine the BBC topology and ratings. Section IV defines the operating region of topology #1. Section V analyzes the capabilities of topology #1 in compensating for the reactive power both without and with the simultaneous drawing/delivery of active power from/to the grid. Section VI extends the analysis to topology #2. Section VII presents a prototypal BBC and reports experimental results relevant to its capabilities of executing the reactive power compensation. Section VIII concludes this paper.

II. Bidirectional Battery Charger

The general single-line block scheme of a three-phase BBC is illustrated in Fig. 1. Its core is the AR. By definition, the AR input and output are its ac and dc sides, respectively; moreover, voltage and current directions at the AR input and output are defined in the way that the power is positive when the battery is charged. On the AR input side, an inductor *L* (or an *LCL* mesh) decouples the AR input voltage v_i from the grid voltage v_g. The inductor comes also useful to filter the high-frequency current harmonics produced by the pulse width modulation (PWM) waveform of v_i so that it can be assumed that the AR input current i_i is sinusoidal. This allows us to neglect the harmonics of v_i and to account only for its fundamental component in expressing the AR input power. The AR output connection differentiates the two BBC topologies. In topology #1, the AR output is directly connected to the battery, apart from the interposition of an *LC* filter that smoothes the battery current. In topology #2, the AR output is connected to the battery through a buck BDDC and, again, an *LC* filter, where BDDC adapts the AR dc output voltage to the battery voltage.

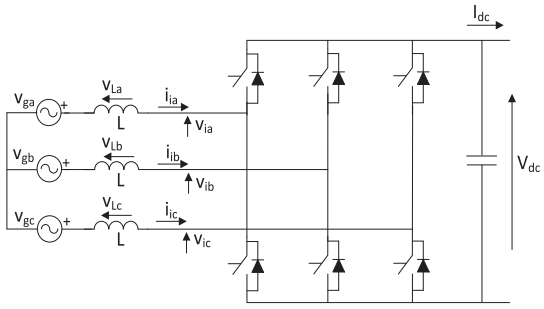

Fig. 2. AR circuital scheme, grid connection included.

The circuital scheme of AR is outlined in Fig. 2. Let the AR line voltages v_{ia}, v_{ib}, and v_{ic} be generated by means of the space vector modulation (SVM) in the linear zone and let V_i be their rms value. By reminding that

1) the upper limit V_u of V_i is

$$V_u = \frac{V_{\rm dc}}{\sqrt{2}\sqrt{3}} = \frac{V_{\rm dc}}{\sqrt{6}} \tag{1}$$

2) V_u must be not less than V_g for the power transitions to be accomplished with the grid.

It follows that the minimum value allowable for $V_{\rm dc}$ is

$$V_{{\rm dc},m} = k\sqrt{6}\, V_g \tag{2}$$

with $k \geq 1$. Selection of k is discussed later on.

Equation (2) leads to the selection of the two BBC topologies. If the minimum voltage of the EV battery exceeds $V_{{\rm dc},m}$, topology #1 is used; otherwise, topology #2 is needed. The minimum voltage of the batteries onboard today's EVs is typically less than $V_{{\rm dc},m}$ in (2), as obtained with a grid voltage of 380 V, and EVs are equipped with BBCs having topology #2. However, topology #1 is still used when charging occurs from enclosures that embed a transformer for insulation purposes, and the transformer steps down the voltage at a suitable level. In this case, V_g in (2) is the output voltage of the transformer.

III. From Battery Specifications to AR Ratings

In charging as well as in delivering power to the grid, current and voltage specifications of the EV battery must be met in order to preserve its performance.

A. Battery Specifications and AR Ratings

Battery charging encompasses two stages, namely the constant current (CC) and the constant voltage (CV), as shown on the left-hand side of Fig. 3. During the CC stage, the battery is charged at the maximum charging current $I_{\rm CC}$ from an initial value of voltage to the maximum value $V_{b,M}$. Let the initial value of voltage be the minimum (or cut off) voltage $V_{b,m}$ of the

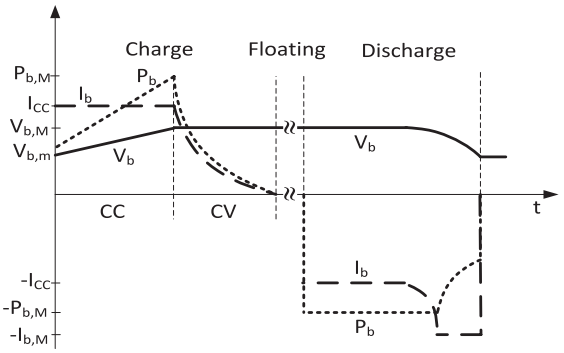

Fig. 3. Diagrams of battery voltage (solid line), battery current (dashed line), and battery power (dotted line) during charging, floating, and discharging.

battery. The voltage ratio

$$\frac{V_{b,M}}{V_{b,m}} = r \tag{3}$$

depends on the battery chemistry but, for both lead-acid and lithium-ion batteries, it is of about 1.4.

At the beginning of the charging process, the power P_b absorbed by the battery is

$$P_{b,m} = V_{b,m} I_{\mathrm{CC}}. \tag{4}$$

During the charging process, the power P_b increases with the battery voltage and reaches its maximum value

$$P_{b,M} = V_{b,M} I_{\mathrm{CC}} = r P_{b,m} \equiv P_R \tag{5}$$

at the completion of the CC stage. Since the charging process is much slower than the thermal dynamics of the AR devices, $P_{b,M}$ sets the rated power P_R of BBC.

The AR current rating is sized for a charging process with unity displacement factor at the grid connection, i.e., with the AR input current i_i in phase with the grid voltage v_g. Then, by disregarding the charger power losses, the active power drawn from the grid is given by

$$P_b = 3 V_g I_i \tag{6}$$

and is equal to the power P_b absorbed by the battery. Being V_g constant, (6) shows that the AR input current I_i is proportional to P_b. At the beginning and the completion of the CC stage, when (4) and (5) hold, the AR input current takes, respectively, the values

$$I_{i,m} = \frac{P_{b,m}}{3V_g} = \frac{V_{b,m} I_{\mathrm{CC}}}{3V_g} \tag{7}$$

$$I_{i,M} = \frac{P_{b,M}}{3V_g} = \frac{V_{b,M} I_{\mathrm{CC}}}{3V_g} = r I_{i,m} \equiv I_R \tag{8}$$

and $I_{i,M}$ sets the rated current I_R of AR.

Once the maximum battery voltage $V_{b,M}$ is reached, the charging process continues with the CV stage; the battery voltage is kept constant at $V_{b,M}$, while the battery current declines to zero. At the completion of the CV stage, according to the V2G paradigm, BBC remains connected to the grid to be ready in assisting it, and the battery is kept charged by the so-called floating charging.

B. Battery Power Delivery

During power delivery, the battery tolerates a maximum discharging current $I_{b,M}$ several times higher than I_{CC}. Let the power delivery process: 1) begin from the condition of fully charged battery, and 2) take place at constant power, equal to P_R. The current that the battery can deliver is restricted by the above-fixed AR ratings I_R and P_R rather than by the battery. Due to them, during the initial power delivery, the maximum current that can be drawn from the battery is I_{CC}. As the power delivery proceeds, the battery voltage decreases and the current drawn from the battery is increased to maintain the power delivery at P_R. In spite of this increase, the AR input current remains constant and equal to I_R. The power delivery continues at rated power until the battery reaches either the minimum voltage $V_{b,m}$ or the maximum current $I_{b,M}$. The diagrams of the battery voltage, current, and power under power delivery are plotted on the right side of Fig. 3 and refer to the situation for which the battery current reaches $I_{b,M}$ before that the battery voltage reaches $V_{b,m}$. Afterwards, the battery current is kept constant at $I_{b,M}$ and the delivered power decreases. When the battery voltage reaches $V_{b,m}$, the power delivery is stopped to prevent the shortening of the battery lifetime.

C. AR Voltage Equations

The voltage equation of the input mesh of one AR phase is

$$\bar{V}_g = \bar{V}_i + \bar{V}_L \tag{9}$$

where $\bar{V}_L$ is the voltage drop across the inductor *L*. Under battery charging with unity displacement factor between $\bar{V}_g$ and $\bar{I}_i$, voltage $\bar{V}_L$ leads $\bar{V}_{\mathrm{g}}$ of $\pi/2$, and the following relationship holds:

$$V_i = \sqrt{{V_g}^2 + {V_L}^2} \tag{10}$$

where V_i is higher than V_g because of the voltage drop V_L. Note that the same relationship as (10) holds under battery power delivery with unity displacement factor, where now $\bar{V}_L$ lags $\bar{V}_g$ of $\pi/2$.

As a role of thumb, the rated value of V_L is set at (11) for the inductor L to reduce the current harmonics injected into the grid at an acceptable level [28]:

$$V_{L,R} = \omega L I_R \cong 0.45\ V_g. \tag{11}$$

By (10) and (11), V_i must be at least equal to

$$V_i = k V_g \qquad k \cong 1.1. \tag{12}$$

By substituting this value of *k* in (2), it is

$$V_{\mathrm{dc},m} \cong 1.1\sqrt{6} V_g = 2.7\ V_g. \tag{13}$$

Equation (13) specifies in a quantitative way the condition for selecting the BBC topology. Indeed, if the minimum voltage $V_{b,m}$ of the EV battery is such that $V_{b,m} \geq V_{\mathrm{dc},m}$, topology #1 is selected since (13) guarantees that both the battery charging from the grid and the battery power delivery to the grid is carried out without the insertion of any BDDC. Otherwise, it is necessary to resort to topology #2.

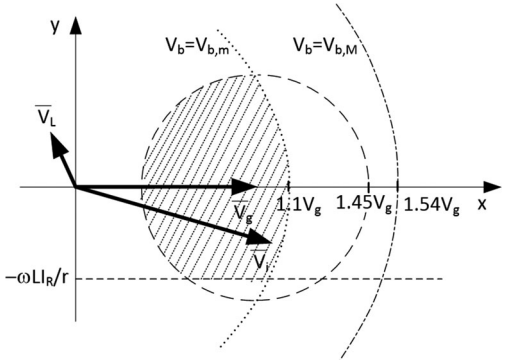

Fig. 4. AR operating limits.

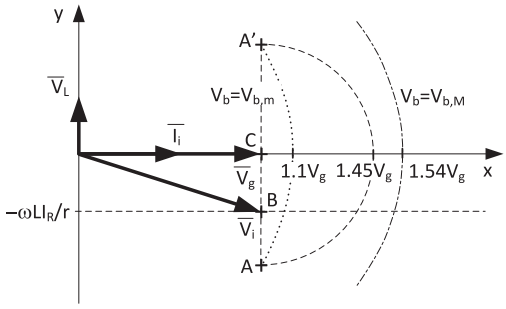

Fig. 5. AR phasor diagram under pure active power exchange.

IV. BBC Topology #1 Operation

Let us analyze at first BBC topology #1 by assuming that $V_{b,m}$ is equal to $V_{\mathrm{dc},m}$. From (3), (8), and (13), I_R can be expressed as

$$I_R \cong 1.1\frac{\sqrt{2}}{\sqrt{3}} r I_{\mathrm{CC}} \cong 1.26\ I_{\mathrm{CC}}. \tag{14}$$

The maximum AR input voltage $V_{i,M}$ is reached when the voltage battery is maximum, i.e., for $V_{\mathrm{dc}} = V_{b,M}$. By (3), $V_{b,M}$ is equal to about $3.78\ V_g$ and $V_{i,M}$ takes the value of

$$V_{i,M} = \frac{V_{b,M}}{\sqrt{6}} \cong 1.54\ V_g \equiv V_R \tag{15}$$

that sets the rated voltage V_R of the AR.

A. BBC Operating Region

When the battery voltage is $V_{b,m}$, the minimum magnitude of the upper limit of $\bar{V}_i$ is achieved, equal to $1.1V_g$, and the vertex of $\bar{V}_i$ describes in the complex *xy* plane a circle of radius $1.1V_g$ having the following equation:

$$V_{i,x}^2 + V_{i,y}^2 = (1.1\ V_g)^2. \tag{16}$$

The circle is plotted with dotted line in Fig. 4, where $\bar{V}_g$ is conveniently set along the axis *x*. By (9), the *x*-, *y*-components of $\bar{V}_i$ for a generic current $\bar{I}_i$ are given by

$$\begin{cases} V_{i,x} = V_g - V_{L,x} \\ V_{i,y} = -V_{L,y} \end{cases} \tag{17}$$

where

$$\begin{cases} V_{L,x} = -\omega L I_{i,y} \\ V_{L,y} = \omega L I_{i,x} \end{cases}. \tag{18}$$

When the battery voltage is $V_{b,M}$, the maximum magnitude of the upper limit of $\bar{V}_i$ is achieved and, by (15), it is equal to $1.54\ V_g$. Correspondingly, the vertex of $\bar{V}_i$ describes in the complex *xy* plane the circle represented by the dash-dotted line in Fig. 4, whose equation is

$$V_{i,x}^2 + V_{i,y}^2 = (1.54\ V_g)^2. \tag{19}$$

Besides operating within the magnitude limitation of $\bar{V}_i$ determined by the battery voltage, the AR must operate within the current rating I_R. In correspondence to I_R, V_L reaches its rated value $V_{L,R}$. By rewriting (17) under this condition, it is

$$(V_{i,x} - V_g)^2 + V_{i,y}^2 = {V_{L,R}}^2. \tag{20}$$

Equation (20) represents I_R in terms of the *x*-, *y*-components of $\bar{V}_i$, and shows that, at rated current, the vertex of $\bar{V}_i$ describes a circle centered in the tip of $\bar{V}_g$ and having radius $V_{L,R}$ given by (11). The circle is plotted with dashed line in Fig. 4.

Since only the active component of $\bar{I}_i$ contributes to the battery-charging current, the battery current specification I_{CC} reflects into a restriction of the active component of $\bar{I}_i$ that, for (8), can be expressed as

$$I_{i,x} \le \frac{V_b I_{\mathrm{CC}}}{3\ V_g} = I_R \frac{V_b}{V_{b,M}}. \tag{21}$$

Equation (21), combined with (17) and (18), poses the following constraint on the *y*-component of $\bar{V}_i$:

$$V_{i,y} \ge -\omega L I_R \frac{V_b}{V_{b,M}}. \tag{22}$$

As a result, the vertex of $\bar{V}_i$ must stay in the half-plane defined by (22) and must be confined between the two circles representative of the current rating and the AR input voltage limitation. The first circle is described by (20), while the other one depends on the actual battery voltage and is comprised between the two circles given by (16) and (19), respectively. Such an area constitutes the BBC operating region; for $V_b = V_{b,m}$, it is tagged by dense lines in Fig. 4.

B. Pure Active Power Exchange

Pure active power exchange means that the only task of BBC is of either charging the battery or withdrawing power from the battery and delivering it to the grid. Under unity displacement factor at the grid connection, the BBC operating point is on the vertical line passing through the vertex of $\bar{V}_{\mathrm{g}}$, as shown in Fig. 5. Moreover, for the AR input current not to exceed the rated value, the operating point must stay on the segment A-A′, where points A and A′ are the intersections of the above-mentioned vertical line with the circle in (20) representing I_R.

Let us consider at first battery charging. At the beginning of the CC stage, the battery voltage is $V_{b,m}$ and (22) can be

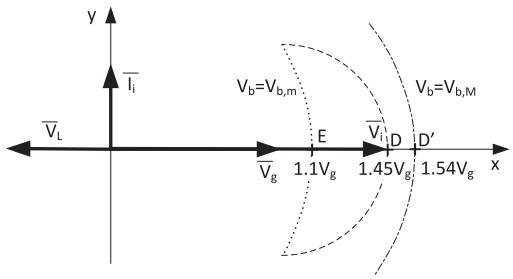

Fig. 6. AR phasor diagram under pure reactive power compensation.

rewritten as

$$V_{i,y} \geq -\omega L I_R \frac{V_{b,m}}{V_{b,M}} = -\omega L \frac{I_R}{r} \cong -0.32\, V_g. \tag{23}$$

Then, the operating point is B whose coordinates are $(V_g,\, -0.32\, V_g)$. As the battery voltage increases, the magnitude of $\bar{I}_i$ increases and the operating point moves toward (and reaches) point A. At this point, I_i gets its rated value I_R, and power P_b absorbed by the battery gets its maximum. From (6), it can be expressed as

$$P_{b,M} = 3\, V_g I_R \equiv P_R \tag{24}$$

and, by the assumption of no losses in BBC, it is equal to P_R. During the CV stage, the battery current declines to nearly zero, and the AR operating point moves from A to C, i.e., to the vertex of $\bar{V}_g$ along the segment A-A′.

Under battery power delivery, executed in agreement with the diagram of Fig. 3, the BBC operating point at the beginning of the process is A′ and remains on A′ until the delivered power is constant. When the delivered power decreases, the operating point moves gradually from A′ toward C along the segment A′-A; as soon as V_b reaches $V_{b,m}$, the operating point jumps steeply to C to avoid over discharging of the battery.

V. Reactive Power Compensation

Being the reactive loads of the grid typically of inductive type, BBC is supposed to compensate for them by absorbing reactive power of capacitive type.

A. Pure Reactive Power Compensation

During pure reactive power compensation, the battery sustains the voltage $V_{\rm dc}$ at the AR dc side but does not deliver any current so that $V_{\rm dc}$ remains constant and, consequently, the compensation could ideally go on indefinitely.

When BBC behaves like a capacitive load, the input current $\bar{I}_i$ leads $\bar{V}_g$ of $\pi/2$, as shown by the phasor diagram of Fig. 6. For a given current, the magnitude of $\bar{V}_i$ is higher than during the active power exchange because $\bar{V}_L$ is in opposition to $\bar{V}_g$ instead of being in quadrature. The maximum reactive power absorbed by BBC occurs under rated AR current and is expressed as

$$Q_M = 3\, V_g I_R \equiv Q_R \tag{25}$$

that sets the rated reactive power Q_R of BBC. Comparison of (25) to (24) shows that Q_R is numerically equal to P_R. The BBC operating point in correspondence of (25) is D of Fig. 6. Indeed, by (9) and (11), the absorption of Q_M requires a magnitude of $\bar{V}_i$ equal to $1.45V_g$. According to (15), this can be obtained even when the battery is not fully charged, as long as V_b is greater than

$$V_b \geq \sqrt{6}\, 1.45\, V_g \cong 3.55\, V_g. \tag{26}$$

When the battery voltage is $V_{b,m}$, the magnitude of $\bar{V}_i$ is limited by (16) and V_L must not exceed $0.1V_g$. This condition is met by reducing the AR input current to $0.22I_R$. Now, the operating point is E of Fig. 6. The reactive power compensated at point E is minimum and is equal to

$$Q_m = 3\, V_g 0.22\, I_R = 0.22\, Q_R. \tag{27}$$

The question can arise on what happens by sizing AR for a current higher than I_R. Inspection of Fig. 6 suggests that this extends the reactive power compensation capabilities of BBC. However, the operating point must remain within the AR input voltage limitation in (19) so that it must not go over D′. At this point, the absorbed reactive power is 1.2 times Q_R and the AR input current is as high as 1.2 times I_R.

B. Convenience of Simultaneous Reactive Power Compensation and Battery Power Exchange

Under battery charging, BBC potentialities are not fully exploited because, for most of the time, AR operates neither at rated current nor under input voltage limitation, being the operating point constrained between points C and A of Fig. 5. The same happens under purely battery power delivery, unless BBC operates at point A′. Then, BBC can be fully exploited by utilizing AR at the rated current or at the input voltage limitation, whenever it is possible. This is attained by executing the reactive power compensation and the battery power exchange simultaneously.

C. Simultaneous Reactive Power Compensation and Battery Charging (CC Stage)

Let us examine at first simultaneous reactive power compensation and battery charging during the CC stage. The AR input current leads the grid voltage of an angle that spans from 0 to $\pi/2$, being the extreme values relevant to pure battery charging and pure reactive power compensation, respectively.

With the initial battery voltage at $V_{b,m}$, the BBC operating point that could fully exploit its capability would be A of Fig. 5, but here the battery-charging current I_b exceeds $I_{\rm CC}$. Hence, to comply with the battery current specification, BBC is operated at point F of Fig. 7, which is located at the intersection of the circle (16) with the line (22), calculated for $V_b = V_{b,m}$. At this point, the *x-, y*-components of $\bar{V}_i$ are

$$\begin{cases} V_{i,x,F} = \sqrt{V_{i,F}^2 - V_{i,y,F}^2} \cong 1.052\, V_g \\ V_{i,y,F} = -V_{L,R} \dfrac{V_{b,m}}{V_{b,M}} \cong -0.32\, V_g \end{cases}. \tag{28}$$

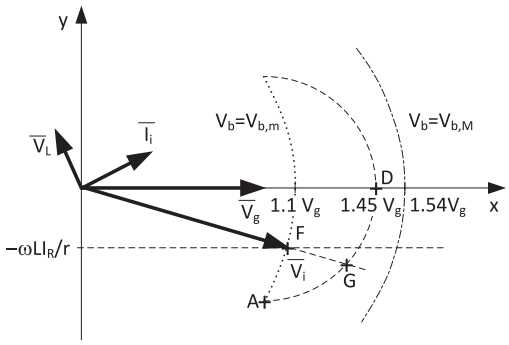

Fig. 7. AR phasor diagram under simultaneous reactive power compensation and battery charging.

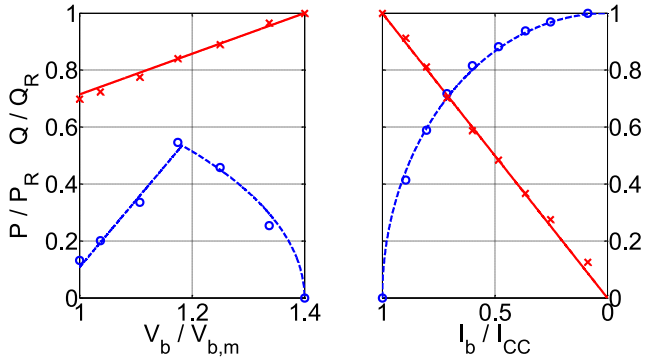

Fig. 8. Active (solid line) and reactive powers (dashed line) absorbed from the grid during CC stage (left) and CV stage (right).

By multiplying V_g by the reactive component $I_{i,y,F}$ of $\bar{I}_i$, which can be derived from (17), (18), and (28), the reactive power absorbed at point F is

$$Q_F = 3\ V_g I_{i,y,F} \cong 0.11\ Q_R. \tag{29}$$

During the CC stage, the active component of $\bar{I}_i$ and the corresponding active power absorbed from the grid increase proportionally to the battery voltage, as expressed by

$$P = 3\ V_g I_{i,x} = V_b I_{\rm CC}. \tag{30}$$

From (17), (18), and (30), the *y*-component of $\bar{V}_i$ turns out to be proportional to $V_{\rm b}$

$$V_{i,y} = -\omega L \frac{V_b I_{\rm CC}}{3\ V_g}. \tag{31}$$

By writing $\bar{V}_i$ in terms of its *x*-, *y*-components and by reminding that, for (1), its upper limit is $V_b/\sqrt{6}$, one obtains

$$V_{i,x}^2 + V_{i,y}^2 = \frac{V_b^2}{6}. \tag{32}$$

Elimination of V_b from (31) and (32) yields (33). It gives the locus of the BBC operating point under simultaneous reactive power compensation and battery charging during the CC stage

$$V_{i,y} = -\frac{\omega L I_{\rm CC}}{\sqrt{\frac{3}{2}V_g^2 - \omega^2 L^2 I_{\rm CC}^2}}\ V_{i,x}. \tag{33}$$

By (33), the operating point moves from F to G along the segment FG. Manipulation of (33) by (5) and (11) leads to the following expression of the locus:

$$V_{i,y} = -\frac{\sqrt{6}V_{L,R}}{\sqrt{V_{b,M}^2 - 6V_{L,R}^2}}\ V_{i,x} \cong -0.30\ V_{i,x}. \tag{34}$$

At point G, the rated current circle is reached. The coordinates of G are

$$\begin{cases} V_{i,x,G} = V_g - \dfrac{6V_{L,R}^2 V_g}{V_{b,M}^2} + V_{L,R} \\ \qquad\qquad \times \sqrt{\left(1 - \dfrac{6V_{L,R}^2}{V_{b,M}^2}\right)\left(1 - \dfrac{6V_g^2}{V_{b,M}^2}\right)} \cong 1.24\ V_g \\ V_{i,y,G} \cong -0.37\ V_g \end{cases}. \tag{35}$$

Then, the AR input voltage and the battery voltage at point G are

$$V_{i,G} = \sqrt{V_{i,x,G}^2 + V_{i,y,G}^2} \cong 1.3\ V_g, \quad V_{b,G} \cong 1.18\ V_{b,m} \tag{36}$$

and the reactive power absorbed from the grid is

$$Q_G = 3\ V_g I_R sin\left[\text{atan}\left(\frac{I_{i,y,G}}{I_{i,x,G}}\right)\right]. \tag{37}$$

By (16) and (17), (37) can be rewritten in the form

$$Q_G = 3\ V_g I_R \sin\left[\text{atan}\left(\frac{V_{i,x,G} - V_g}{V_{i,y,G}}\right)\right] \cong 0.53\ Q_R. \tag{38}$$

When the battery voltage increases beyond $V_{b,G}$, the operating point can no longer stay on the locus (34), otherwise the AR input current would exceed I_R. Instead, it moves along the rated current circle up to reach point A when the battery voltage becomes $V_{b,M}$. At this point, only pure battery charging is executed. From here on, battery charging enters into the CV stage and the applicable analysis is presented in next section.

The BBC capabilities in terms of battery-charging power and reactive power compensation during the CC stage, normalized to P_R and Q_R, respectively, are plotted on the left-hand side of Fig. 8 as a function of the battery voltage normalized to $V_{b,m}$.

D. Simultaneous Reactive Power Compensation and Battery Charging (CV Stage)

During the CV stage, the active power absorbed by the battery is $V_{b,M} I_b$. It decreases linearly with I_b. As I_b decreases, an increasing amount of reactive current can be absorbed from the grid by keeping the magnitude of $\bar{I}_i$ constant at the rated value. The BBC operating point moves along the rated current circle from A to D of Fig. 7. In correspondence, the compensated reactive power is

$$Q_{\rm CV} = \sqrt{9V_g^2 I_R^2 - V_{b,M}^2 I_b^2}. \tag{39}$$

At the completion of the CV stage, I_b is 0 and Q reaches the rated value Q_R. From here one, floating charging of the battery occurs and BBC can compensate for a reactive power equal to Q_R.

The BBC capabilities in terms of battery-charging power and reactive power compensation during the CV stage, normalized

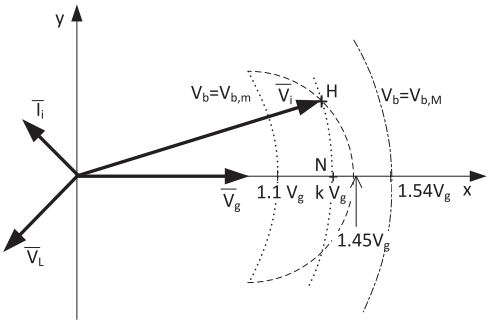

Fig. 9. AR phasor diagram under simultaneous reactive power compensation and battery power delivery.

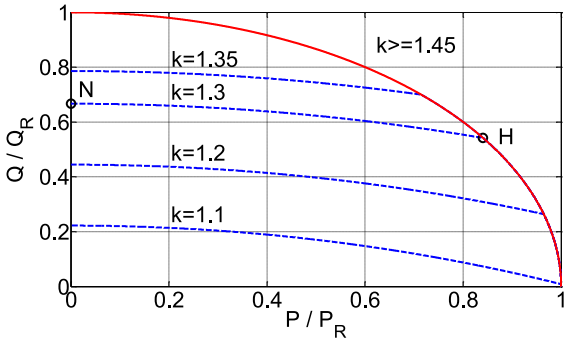

Fig. 10. Reactive power compensation versus battery power delivery under AR rated current (solid line) and input voltage limitation (dashed lines) for different values of *k*.

to P_R and Q_R, respectively, are plotted on the right-hand side of Fig. 8 as a function of the battery current normalized to $I_{\rm CC}$.

E. Simultaneous Reactive Power Compensation and Battery Power Delivery

Under battery power delivery, the BBC operating point is constrained by the AR current rating and the magnitude limitation for $\bar{V}_i$, as explained in Section IV-A. If (26) holds, i.e., for the magnitude of $\bar{V}_i$ greater than $1.45V_g$, AR can operate in any point of the rated current circle. Therefore, any simultaneous combination of reactive power compensation and active power delivery can take place, provided that (40) is fulfilled

$$\sqrt{P^2+Q^2}=P_R. \tag{40}$$

As the battery voltage decreases below $3.55V_g$, BBC operates at the rated current only when $\bar{I}_i$ is nearly in opposition to $\bar{V}_g$, otherwise AR is subjected to the magnitude limitation for $\bar{V}_i$, as shown in Fig. 9. Under such a limitation, the AR input current is lower than the rated one and the operating point stays on the circle of equation

$$V_{i,x}^2+V_{i,y}^2=k^2V_g^2 \tag{41}$$

where $1.1\le k\le 1.45$. The operating point passes from the AR rated current circle to the AR input voltage limitation circle at point H of Fig. 9; this point is the intersection of the circles (20) and (41) and has the following coordinates:

$$\begin{cases} V_{i,x,H}=\dfrac{V_g^2\left(1+k^2\right)-V_{L,R}^2}{2\,V_g} \\ V_{i,y,H}=\sqrt{-\dfrac{V_g^2\left(1-k^2\right)^2}{4}-\dfrac{V_{L,R}^4}{4V_g^2}+\dfrac{\left(1+k^2\right)V_{L,R}^2}{2}}. \end{cases} \tag{42}$$

By multiplying V_g by the reactive component of $\bar{I}_i$ in H, which can be derived from (17), (18), and (42), the reactive power absorbed at point H can be expressed as

$$Q_H=\frac{Q_R\,V_g}{V_{L,R}}\frac{1}{2}\left[\left(k^2-1\right)-\frac{V_{L,R}^2}{V_g^2}\right]\cong Q_R\frac{k^2-1.2}{0.9}. \tag{43}$$

The corresponding active power delivered to the grid is

$$P_H=\sqrt{P_R^2-Q_H^2}. \tag{44}$$

When the operating point is on the AR input voltage limitation circle, the relationship between reactive and active powers, as derived in Appendix I, is

$$Q=\frac{Q_RV_g}{V_{L,R}}\left(\sqrt{k^2-\frac{V_{L,R}^2}{V_g^2}\frac{P^2}{P_R^2}}-1\right). \tag{45}$$

The maximum of the reactive power compensation is reached at point N of Fig. 9. It is readily calculated from (45) by equating *P* to zero, yielding

$$Q_N=\frac{Q_RV_g}{V_{L,R}}\left(k-1\right)\cong 2.22\,Q_R\left(k-1\right). \tag{46}$$

By inspection of Fig. 9 it appears that the *x*-component of $\bar{V}_L$ is greater in point N than in H. Consequently, the reactive component of $\bar{I}_i$ in N exceeds that one in H, and Q_N is higher than Q_H even if the magnitude of $\bar{I}_i$ is lower. This outcome is confirmed by the graphs of Fig. 10, which give the available combinations of battery power delivery and reactive power compensation under AR current rating (with solid line) or AR input voltage limitation (with dashed lines). The figure reports four different values of k for BBC operating under AR input voltage limitation as well as the operating points N and H for $k=1.3$. By (12), k can be at least equal to 1.1 for the battery to deliver power to the grid. However, if $k=1.1$ and the battery continues to deliver power, its voltage decreases below $V_{b,m}$ so that k decreases below 1.1. Thus, for $k=1.1$, BBC can execute only reactive power compensation, being Q equal to $0.22Q_R$ as per graphs of Fig. 10 and the result in (27).

VI. BBC Topology #2 Operation

If the minimum battery voltage is lower than $V_{{\rm dc},m}$ in (2), BDDC is placed between the AR dc side and the EV battery, as shown in Fig. 11, to adapt the AR dc output voltage to the battery. The AR keeps the dc-link voltage $V_{\rm dc}$ at a constant value, while BDDC regulates the battery current/voltage during the CC/CV stage under charging and the battery power/current under power delivery.

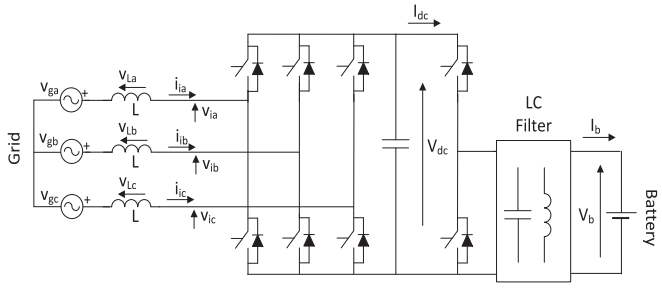

Fig. 11. BBC topology #2 with BDDC.

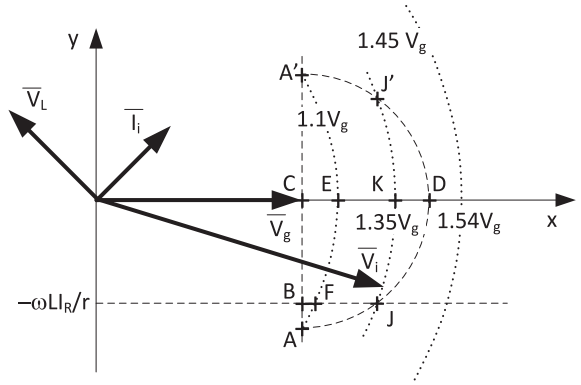

Fig. 12. AR phasor diagram under simultaneous reactive power compensation and battery power exchange with fixed dc-side voltage.

A. Comparison Settings

For a fair comparison of the capabilities of the two BBC topologies, the same values are taken for:

1) the rated power and the ratio r of the battery,
2) the AR rated current as given by (8),
3) the AR rated voltage as given by (15).

With topology #2, the AR dc output voltage $V_{\rm dc}$ is no more related to the battery voltage and, in principle, can be as high as one wishes. However, the constraints posed by the setting 3) above and (10) restrict the amplitude of $V_{\rm dc}$ in the interval going from (13) to *r* times (13). This means that the minimum and maximum values allowed for $V_{\rm dc}$ are

$$\begin{cases} V_{{\rm dc},m} = 2.7\ V_g \\ V_{{\rm dc},M} = 3.78\ V_g \end{cases}. \tag{47}$$

They coincide with the values taken by $V_{\rm dc}$ in topology #1 in correspondence to $V_{b,m}$ and $V_{b,M}$.

Topology #2 operates correctly only if $V_{\rm dc}$ exceeds the battery voltage in any working condition. Consequently, the maximum voltage $V_{b,M,\#2}$ allowed for the battery is

$$V_{b,M,\#2} = \frac{V_{{\rm dc},m}}{q}, \quad q \geq 1 \tag{48}$$

where subscript #2 denotes a quantity referred to topology #2. By reminding that $V_{{\rm dc},m}$ in topology #1 coincides with $V_{b,m}$, substitution of (3) into (48) yields

$$V_{b,M,\#2} = \frac{V_{b,M}}{qr}. \tag{49}$$

According to setting 1) above, the rated power of the battery for topology #2 is equal to that of topology #1. Then, by (49), its maximum charging current is

$$I_{{\rm CC},\#2} = qrI_{\rm CC}. \tag{50}$$

From (49) and (50), it emerges that the curves of voltage, current, and power of the battery in topology #2 under charging and power delivery are the same as in Fig. 3, except for the magnitudes of voltage and current that are *qr* times lower and higher, respectively.

B. BBC Operation

The BDDC presence does not affect the current and voltage quantities involved in AR so that the phasor diagrams of Figs. 5, 6, and 9, collected together in Fig. 12, still hold, the only difference being that the radius of the circle representing the AR input voltage limitation does not change with the battery voltage. Like in topology #1, the AR current rating imposes that the BBC operating points stay within the circle (20), while the battery-charging current specification imposes that the BBC operating points stay in the half-plane above the horizontal line of ordinate $-\omega LI_R/r$.

Under pure active power exchange, BBC operates irrespectively from $V_{\rm dc}$, provided that i) its value is within the fork in (47) and ii) (48) is met. Then, the BBC behavior is the same as that described in Section IV-B. Under pure reactive power compensation, the maximum reactive power compensation ranges from Q_m, when $V_{\rm dc}$ is equal to $V_{{\rm dc},m}$, to Q_R, when $V_{\rm dc}$ is increased up to $3.55V_{\rm g}$ and AR is run at the rated current. Under simultaneous reactive power compensation and battery power exchange, BBC operation is depending on the selected value of $V_{\rm dc}$. Three working hypotheses are discussed below, namely the minimum voltage solicitations, the AR current rating exploitation, and a mixed solution.

C. Minimum Voltage Solicitations

The first hypothesis is intended to minimize the voltage solicitations across AR and BDDC by setting $V_{\rm dc}$ at $V_{{\rm dc},m}$ in (47), i.e., at $2.7V_g$. Consequently, in Fig. 12, the circle relevant to the AR input voltage limitation has radius of $1.1V_g$.

Under simultaneous reactive power compensation and battery charging, the BBC operating point at the beginning of the CC stage is F in order that the battery-charging current does not exceed $I_{{\rm CC},\#2}$. As it happened for topology #1, at point F, the active component of $\bar{I}_i$ is equal to I_R/r and the reactive power absorbed from the grid is equal to (29). While the battery voltage increases, the operating point moves toward A along the circle of the AR input voltage limitation. Point A is reached at the end of the CC stage, where the reactive power absorbed from the grid is zero. During the CV stage, the operating point moves from A toward E along the same circle. Point E is reached when the battery is fully charged. At this point, the absorbed reactive power is given by Q_m, i.e., by $0.22Q_R$ as found in (27). It is worth to note that Q_m represents the maximum reactive power that is compensated for under the working hypothesis

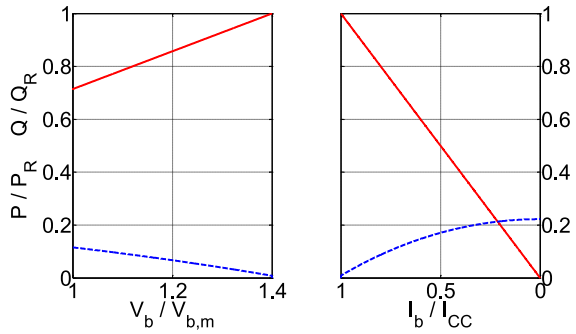

Fig. 13. Active (solid line) and reactive powers (dashed line) absorbed from the grid during CC stage (left) and CV stage (right) with $V_{\rm dc} = 2.7V_g$.

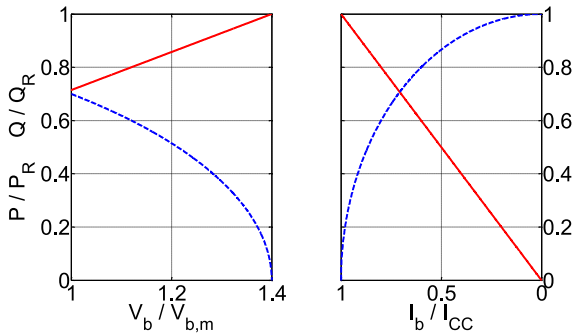

Fig. 14. Active (solid line) and reactive powers (dashed line) absorbed from the grid during CC stage (left) and CV stage (right) with $V_{\rm dc} = 3.55V_g$.

of $V_{\rm dc} = V_{{\rm dc},m}$. According to this hypothesis, BBC operates under AR input voltage limitation along the full battery-charging process, while it operates under AR current rating only at point A. The BBC capabilities in terms of battery-charging power and reactive power compensation during the CC and CV stages with $V_{\rm dc} = 2.7V_g$ are plotted in Fig. 13.

Simultaneous reactive power compensation and battery power delivery can be executed at any operating point on the arc E-A′ and can go on as long as the battery discharges at $V_{b,m}$.

D. AR Current Rating Exploitation

The second hypothesis is intended to fully exploit the AR current rating by setting $V_{\rm dc}$ at

$$V_{\rm dc} = 1.45\sqrt{6}\ V_g \cong 3.55\ V_g \tag{51}$$

so that the rated current circle is entirely within the circle of the AR input voltage limitation, here given by

$$V_{i,x}^2 + V_{i,y}^2 = (1.45\ V_g)^2. \tag{52}$$

This feature is attained at the expenses of voltage solicitations across AR and BDDC that are $3.55/2.7 \cong 1.3$ times higher than with the first hypothesis.

Operating at rated current, a higher reactive power is compensated for. Indeed, the BBC operating point moves along the arc that goes from point J to A during the CC stage, and from point A to D during the CV stage. The BBC capabilities in terms of battery-charging power and reactive power compensation during the CC and CV stages under this hypothesis are plotted in Fig. 14. Comparison of Fig. 14 with Fig. 8 shows that keeping $V_{\rm dc}$ constant at $3.55\ V_g$ makes BBC able to compensate for a larger amount of reactive power during the first part of the CC stage.

From Fig. 12, one can recognize that any operating point outside the circle of the AR input voltage limitation exceeds the AR rated current. Consequently, there is no advantage in increasing $V_{\rm dc}$ beyond $3.55\,V_g$. This entails that AR can be sized for a voltage a bit lower than with topology #1, where $V_{b,M}$ – and hence $V_{\rm dc}$ – was $3.77V_g$.

Simultaneous reactive power compensation and battery power delivery can be executed at any operating point on the arc D-A′ of the circle of the AR rated current.

E. Mixed Solution

The third hypothesis is intended to make AR functioning at rated current during the CC stage of the battery charging, and under input voltage limitation during the CV stage. Such a solution appears a good compromise between reactive power compensation and voltage solicitations across AR and BDDC. It is implemented by selecting $V_{\rm dc}$ so that the circle of the AR input voltage limitation, the line of the battery current limit, and the circle of the rated current intersect all together in point J. By this hypothesis, the operating point moves from J to A during the CC stage. During the first part of the CV stage, the operating point moves back to J by maintaining the current at the rated value; then, the CV stage is completed with the operating point that moves to K along the circle of the AR input voltage limitation.

The coordinates of point J are determined by solving the system of equations composed by (20), (23), and (41). It turns out that the coordinates of J are

$$\begin{cases} V_{i,x,J} = V_g + V_{L,R}\sqrt{1 - \dfrac{1}{r^2}} \cong 1.31\ V_g \\ V_{i,y,J} = -\dfrac{V_{L,R}}{r} \cong -0.32\ V_g \end{cases} \tag{53}$$

and that the required value of $V_{\rm dc}$ is

$$V_{{\rm dc},J} = 1.35\sqrt{6}V_g \cong 3.31\ V_g. \tag{54}$$

Note that this value is about 1.23 times higher than with the first hypothesis and about 1.07 less than with the second hypothesis. In practice, it is hard to keep BBC operating exactly at point J so that it is of interest to describe the BBC behavior around that point. This is addressed in Appendix II.

At point J, the battery-charging power and the reactive power compensation are

$$P_J = \frac{P_M}{r} \cong 0.71\ P_M \tag{55}$$

$$Q_J = Q_M\sqrt{1 - \frac{1}{r^2}} \cong 0.69\ Q_M. \tag{56}$$

The maximum reactive power is absorbed at point K and its value, obtained by help of (54), is about $0.77Q_{\rm R}$. The BBC capabilities in terms of battery-charging power and reactive power

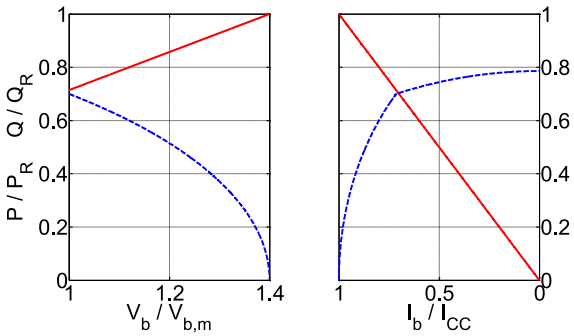

Fig. 15. Active (solid line) and reactive powers (dashed line) absorbed from the grid during CC stage (left) and CV stage (right) with $V_{\rm dc} = 3.31 V_g$.

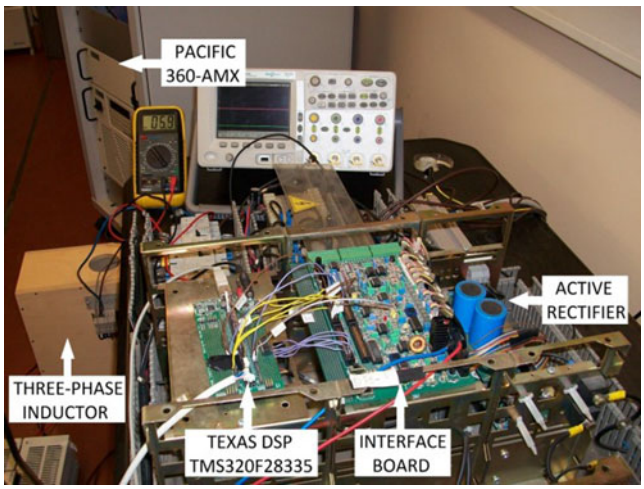

Fig. 16. Prototypal BBC arrangement.

compensation during the CC and CV stages with $V_{\rm dc} = 3.31\ V_g$ are plotted in Fig. 15. As expected, the reactive power takes values in between those of Figs. 13 and 14.

Simultaneous reactive power compensation and battery power delivery can be executed at any operating point on the trajectory K-J′-A′.

VII. Experimental Results

A prototypal BBC with topology #1 has been set up to check the theoretical findings; a picture of it is shown in Fig. 16. BBC utilizes a three-phase current-controlled AR built around an IGBT module 6MBI10S-120 of Fuji Electrics having rated voltage of 1200 V and maximum continuous current of 10 A. A Texas DSP TMS320F28335 samples the grid voltages, the AR input currents, and the magnitude and phase references of the AR input currents by help of an on-purpose built interface board, and applies the gate commands to the IGBTs. Grid voltages and AR input currents are detected by sensors produced by LEM having part numbers LV25-400 and LTS15 NP, respectively. The PWM frequency and the sampling rate of the DSP have been fixed at 10 kHz. The control program, whose execution frequency is also of 10 kHz, has been developed in the Code Composer environment using the C language and implemented

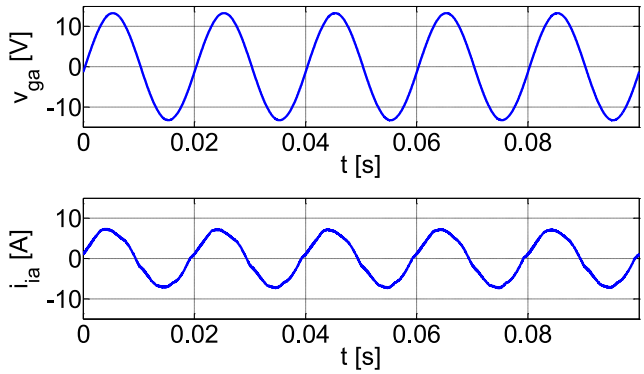

Fig. 17. Grid voltage and AR input current at point F.

in the DSP firmware. The control routines work in a stationary frame synchronized to the grid voltage and adjust magnitude and phase of the AR input currents according to the references imposed by the user through two potentiometers. The adjustment is accomplished by means of two PI regulators whose outputs are processed to calculate the IGBT duty-cycles according to the SVM method and by forwarding the duty cycles to the PWM module of DSP. The firmware checks if SVM is about to enter into overmodulation and reports this circumstance by a digital output signal to indicate that AR is operating under input voltage limitation. The filter decoupling AR from the grid is a three-phase inductor of 3 mH. The EV battery consists of four 12-V 100-Ah lead-acid modules and its voltage ranges from 40 to 56 V, being 48 V the rated value; the maximum charging current is C/10, i.e., 10 A. However, $I_{\rm CC}$ has been set at 5.5 A to fulfill the current ratings of the available AR power switches. To agree with the battery voltages, BBC has been connected to a programmable power source, specifically the Pacific 360-AMX, which acts as a low-voltage three-phase grid. Since the Pacific 360-AMX manages unidirectional power flows, only tests relevant to the battery charging have been carried out.

A digital oscilloscope TDS5034 of Tektronix acquires the grid voltage and the AR input current of the phase a by means of suitable probes as well as the digital signal of the input voltage limitation outputted by DSP. Battery voltage and current are monitored by hand-held multimeters.

The trajectory F-G-A of Fig. 7 has been explored during the CC stage of battery charging. A number of tests have been executed while the battery voltage was increasing. Each test consisted in adjusting magnitude and phase of the AR input current in order to keep the battery-charging current constant at 5.5 A and to meet the condition of AR input voltage limitation. Grid voltage and AR input current have been picked up by the digital oscilloscope at a rate of 500 kS/s and the samples have been stored in a PC for subsequent processing to determine the active and reactive powers. The grid voltage and the AR input current relevant to point F are plotted in Fig. 17; as expected, the AR input current is lower than the rated one and slightly leads the grid voltage. Point G has been detected when the AR input voltage limitation occurred concurrently with a magnitude of the AR input current equal to its rated value. The grid voltage and the AR input current relevant to point G are plotted in Fig. 18;

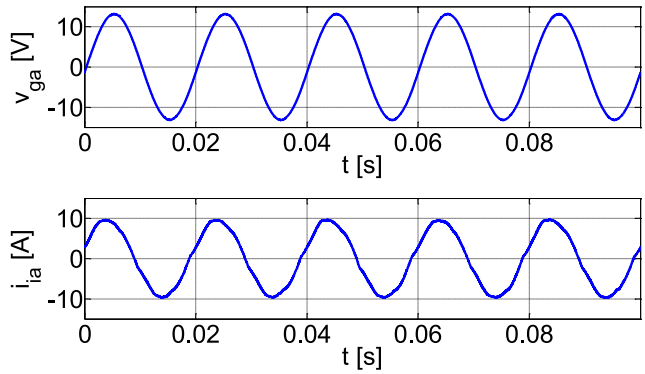

Fig. 18. Grid voltage and AR input current at point G.

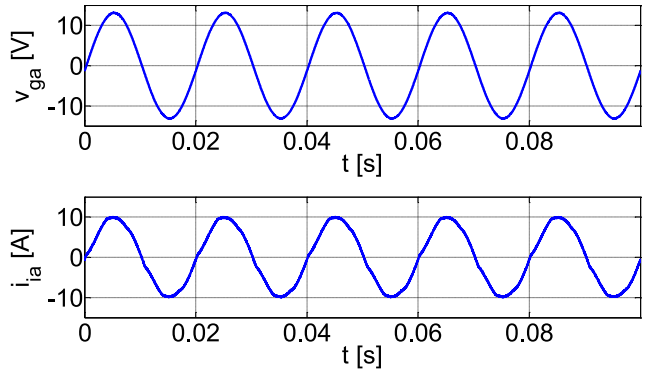

Fig. 19. Grid voltage and AR input current at point A.

here, the phase advance of the AR input current with respect to the grid voltage is higher. Then, tests have been executed by maintaining the magnitude of the AR input current at its rated value and by adjusting its phase angle in order to keep the battery-charging current constant at 5.5 A during the increase of the battery voltage. Point A has been detected when the battery voltage has arrived at 56 V. The corresponding plots of the grid voltage and the AR input current are shown in Fig. 19; in this condition, the maximum active power is injected in the battery, and, hence, the current is in phase with the grid voltage.

The A-G-D trajectory of Fig. 7 has been explored during the CV stage of battery charging. The relevant tests have been executed by maintaining the AR input current at the rated magnitude and by adjusting its phase angle in order to gradually reduce the battery current until it has went down at 0.5 A, i.e., at 0.1 I_{CC}. Fig. 20 shows the grid voltage and the AR input current at point D, where the current leads the grid voltage of $\pi/2$.

First harmonic magnitudes of the grid voltage and the AR input current, and the angular displacement between them have been worked out by processing the samples acquired from the oscilloscope by means of a Fourier analysis-based program written in the MATLAB environment. From the values of the magnitudes and the displacement, the active and reactive powers absorbed by BBC have been computed; they result in fully agreement with the theoretical findings of Section V, as confirmed by Fig. 8, where theoretical and experimental results are reported. In the figure, the experimental data of the active power

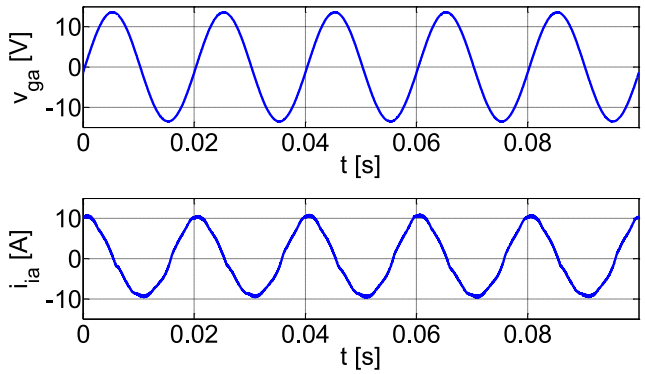

Fig. 20. Grid voltage and AR input current at point D.

are marked with a cross while those of the reactive power by a circle.

VIII. Conclusion

This paper has investigated the capabilities of a V2G-enabled EV in executing the reactive power compensation. After establishing the ratings of BBC by tailoring it to the characteristics of the battery onboard a given EV, two BBC topologies have been envisaged depending on the minimum level of the battery voltage with respect to the grid voltage. For the two topologies, different tasks have been examined, namely the pure exchange of active power with the grid, the pure compensation of reactive power, and the simultaneous exchange of active power and compensation of reactive power. The maximum amount of reactive power that BBC is able to manage as a function of the state of charge of the battery has been calculated with the help of the phasor diagrams. Key operating points of BBC have been identified in the phasor plane in correspondence of the transition of the operation of AR embedded in BBC from rated current to input voltage limitation and vice versa. Finally, a prototypal BBC has been set up and subjected to experimental tests to obtain the maximum active and reactive powers absorbed by it during the battery charging, showing that the obtained power values fully agree with the theoretical findings.

Appendix I

The derivation of (45) is explicated below. Substitution of (17) into (18) leads to the following *x*-, *y*-components of the AR input voltage:

$$\begin{cases} V_{i,x} = V_g + \omega L I_{i,y} \\ V_{i,y} = -\omega L I_{i,x} \end{cases}. \tag{A.1}$$

Thanks to (A.1), (41) can be expressed as

$$V_g^2 + (\omega L I_{i,y})^2 + 2\, V_g\, (\omega L I_{i,y}) + (\omega L I_{i,x})^2 = k^2 V_g^2. \tag{A.2}$$

By multiplying and dividing by $3V_g I_R$ the terms within the round brackets of (A.2), it can be rewritten in the form

$$V_g^2 + \left(\frac{V_{L,R} Q}{Q_M}\right)^2 + 2\, V_g \frac{V_{L,R} Q}{Q_M} + \left(\frac{V_{L,R} P}{P_M}\right)^2 = k^2 V_g^2 \tag{A.3}$$

and then in the form

$$\left(V_g + \frac{V_{L,R}Q}{Q_M}\right)^2 = V_g^2\left[k^2 - \left(\frac{V_{L,R}P}{V_g P_M}\right)^2\right]. \qquad \text{(A.4)}$$

By making Q explicit in (A.4), (45) is obtained.

APPENDIX II

It is reasonable to assume that the main BBC task around point J is to charge the battery with the maximum battery-charging current. Therefore, the principal action of the BBC control system is devoted at keeping the BBC operating point on the horizontal line of ordinate $-\omega L\frac{I_R}{r}$ by regulating the active component of $\bar{I}_i$. As a secondary action, it increases the reactive component of $\bar{I}_i$ until either the AR current rating or the AR input voltage limitation is reached. Let us now consider that the AR current rating is reached first. This means that the actual operating point is on the right of the theoretical position of point J, due, for instance, to the fact that the actual $V_{\rm dc}$ is higher than $1.35V_g$ or the current rating is too low to fully utilize the AR input voltage limitation. Let us now consider that the AR input voltage limitation is reached first. This means that the actual operating point is on the left of the theoretical position of point J, due, for instance, to the fact that the actual $V_{\rm dc}$ is less than $1.35V_{\rm g}$ or the current rating is too high with respect to the AR input voltage limitation.

REFERENCES

[1] M. Kesler, M. C. Kisacikoglu, and L. M. Tolbert, "Vehicle-to-grid reactive power operation using plug-in electric vehicle bidirectional offboard charger," *IEEE Trans. Ind. Electron.*, vol. 61, no. 12, pp. 6778–6784, Dec. 2014.

[2] A. Anwar, F. R. Islam, A. B. M. Nasiruzzaman, and H. R. Pota, "Design a unified power quality conditioner using V2G technology," in *Proc. IEEE Int. Power Eng. Optim. Conf.*, 2012, pp. 521–526.

[3] M. Yilmaz and P. T. Krein, "Review of the impact of vehicle-to-grid technologies on distribution systems and utility interfaces," *IEEE Trans. Power Electron.*, vol. 28, no. 12, pp. 5673–5689, Dec. 2013.

[4] S. Bai and S. M. Lukic, "Unified active filter and energy storage system for an MW electric vehicle charging station," *IEEE Trans. Power Electron.*, vol. 28, no. 12, pp. 5793–5803, Dec. 2013.

[5] S. Haghbin, S. Lundmark, M. Alakula, and O. Carlson, "Grid-connected integrated battery chargers in vehicle applications: Review and new solution," *IEEE Trans. Ind. Electron.*, vol. 60, no. 2, pp. 459–473, Feb. 2013.

[6] K. Bao, S. Li, and H. Zhenh, "Battery charge and discharge control for energy management in EV and utility integration," in *Proc. Power Energy Soc. Gen. Meet.*, 2012, pp. 1–8.

[7] T. N. Pham, H. Trinh, and L. V. Hien, "Load frequency control of power systems with electric vehicles and diverse transmission links using distributed functional observers," *IEEE Trans. Smart Grid*, vol. 7, no. 1, pp. 238–252, Jan. 2016.

[8] E. L. Karfopoulos and N. D. Hatziargyriou, "Distributed coordination of electric vehicles providing V2G services," *IEEE Trans. Power Syst.*, vol. 31, no. 1, pp. 329–338, Jan. 2016.

[9] J. Popović-Gerber *et al.*, "Power electronics enabling efficient energy usage: Energy savings potential and technological challenges," *IEEE Trans. Power Electron.*, vol. 27, no. 5, pp. 2338–2353, May 2012.

[10] G. Byeon, T. Yoon, S. Oh, and G. Jang, "Energy management strategy of the DC distribution system in buildings using the EV service model," *IEEE Trans. Power Electron.*, vol. 28, no. 4, pp. 1544–1554, Apr. 2013.

[11] M. C. Kisacikoglu, B. Ozpineci, and L. M. Tolbert, "EV/PHEV bidirectional charger assessment for V2G reactive power operation," *IEEE Trans. Power Electron.*, vol. 28, no. 12, pp. 5717–5727, Dec. 2013.

[12] M. Kazerani and N. Wong, "A review of bidirectional on-board charger topologies for plugin vehicles," in *Proc. 25th IEEE Can. Conf. Electr. Comput. Eng.*, 2012, pp. 1–6.

[13] M. Yilmaz and P.T. Krein, "Review of battery charger topologies, charging power levels, and infrastructure for plug-in electric and hybrid vehicles," *IEEE Trans. Power Electron.*, vol. 28, no. 5, pp. 2151–2169, May 2013.

[14] M. Su, H. Wang, Y. Sun, J. Yang, W. Xiong, and Y. Liu, "AC/DC matrix converter with an optimized modulation strategy for V2G applications," *IEEE Trans. Power Electron.*, vol. 28, no. 12, pp. 5736–5745, Dec. 2013.

[15] I. Subotic, N. Bodo, and E. Levi, "Single-phase on-board integrated battery chargers for EVs based on multiphase machines," *IEEE Trans. Power Electron.*, vol. 31, no. 9, pp. 6511–6523, Sep. 2016.

[16] M. A. Khan, I. Husain, and Y. Sozer, "Integrated electric motor drive and power electronics for bidirectional power flow between the electric vehicle and DC or AC grid," *IEEE Trans. Power Electron.*, vol. 28, no. 12, pp. 5774–5783, Dec. 2013.

[17] O. Hegazy, R. Barrero, J. Van Mierlo, P. Lataire, N. Omar, and T. Coosemans, "An advanced power electronics interface for electric vehicles applications," *IEEE Trans. Power Electron.*, vol. 28, no. 12, pp. 5508–5521, Dec. 2013.

[18] U. K. Madawala and D. J. Thrimawithana, "A bidirectional inductive power interface for electric vehicles in V2G systems," *IEEE Trans. Ind. Electron.*, vol. 58, no. 10, pp. 4789–4796, Oct. 2011.

[19] S. Weearsinghe, D. J. Thrimawithana, and U. K. Madawala, "Modeling bidirectional contactless grid interfaces with a soft DC-link," *IEEE Trans. Power Electron.*, vol. 30, no. 7, pp. 3528–3541, Jul. 2015.

[20] M. P. Theodoridis, "Effective capacitive power transfer," *IEEE Trans. Power Electron.*, vol. 27, no. 12, pp. 4906–4913, Dec. 2012.

[21] T. S. Ustun, A. Zayegh, and C. Ozansoy, "Electric vehicle potential in Australia: Its impact on smart grids," *IEEE. Ind. Electron. Mag.*, vol. 7, no. 4, pp. 15–25, Dec. 2013.

[22] S. S. Williamson, A. K. Rathore, and F. Musavi, "Industrial electronics for electric transportation: Current state-of-the-art and future challenges," *IEEE Trans. Ind. Electron.*, vol. 62, no. 5, pp. 3021–3032, May 2015.

[23] D. T. Shahani, B. Singh, and A. K. Verma, "Grid to vehicle and vehicle to grid energy transfer using single-phase bidirectional AC-DC converter and bidirectional DC-DC converter," in *Proc. Int. Conf. Energy, Autom., Signal*, 2011, pp. 1–5.

[24] M. C. Kisacikoglu, B. Ozpineci, and L. M. Tolbert, "Effects of V2G reactive power compensation on the component selection in an EV or PHEV bidirectional charger," in *Proc. IEEE Energy Convers. Congr. Expo.*, 2010, pp. 870–876.

[25] Z. Shu, S. Xie, and Q. Li, "Single-phase back-to-back converter for active power balancing, reactive power compensation, and harmonic filtering in traction power system," *IEEE Trans. Power Electron.*, vol. 26, no. 2, pp. 334–343, Feb. 2011.

[26] C. Silvestre, D. M. Sousa, and A. Roque, "Reactive power compensation using on board stored energy in electric vehicles," in *Proc. Annu. Conf. IEEE Ind. Electron. Soc.*, 2012, pp. 5227–5232.

[27] M. C. Kisacikoglu, M. Kesler, and L. M. Tolbert, "Single-phase on-board bidirectional PEV charger for V2G reactive power operation," *IEEE Trans. Smart Grid*, vol. 6, no. 2, pp. 767–775, Mar. 2015.

[28] H. Mao, F. C. Y. Lee, D. Boroyevich, and S. Hiti, "Review of high-performance three-phase power-factor correction circuits," *IEEE Trans. Ind. Electron.*, vol. 44, no. 4, pp. 437–446, Aug. 1997.

Giuseppe Buja (M'75–SM'84–F'95–LF'13) received the "Laurea" (Hons.) degree in power electronics engineering from the University of Padova, Padova, Italy, in 1970.

He is currently a Full Professor with the University of Padova. His scientific interests include power and industrial electronics. His current research interests include wired and wireless charging of electric vehicles, and power conversion systems for renewable energies.

Dr. Buja received the IEEE Industrial Electronics Society (IES) Eugene Mittelmann Achievement Award "in recognition of his outstanding technical contributions to the field of industrial electronics," and the Best Paper Award from the IEEE TRANSACTIONS ON INDUSTRIAL ELECTRONICS in 2016. He has served the IEEE in several capacities, including as the General Chairman of the *20th Annual Conference of the IES (IECON)* in 1994. He is currently an Associate Editor of the IEEE TRANSACTIONS ON INDUSTRIAL ELECTRONICS, a Member of the Editorial Board of the *Chinese Journal of Electrical Engineering*, and a Senior Member of the Administrative Committee of the IES.

Manuele Bertoluzzo received the M.S. degree in electronic engineering and the Ph.D. degree in industrial electronics and computer science from the University of Padova, Padova, Italy, in 1993 and 1997, respectively.

From 1998 to 2000, he was a Member in the Research and Development Division of an electric drive factory.

In 2000, he joined the Department of Electrical Engineering, University of Padova, as a Researcher in the Scientific Disciplines' Group "electric converters, machines, and drives." Since 2015, he is an Associate Professor of Systems for Automation and of Electric Road Vehicle for graduate students. He is currently involved in the analysis and design of power electronics and control systems for wireless power transfer systems.

Christian Fontana (M'16) received the B.S. and M.S. degrees in electric engineering from the University of Padova, Padova, Italy, in 2010 and 2013, respectively, where since 2014, he has been working toward the Ph.D. degree in the Department of Industrial Engineering.

His Ph.D. activities are devoted to the analysis and the control of solid-state transformers, with specific attention to the isolated dc–dc converter stage. His research interests include power electronics circuits and control systems for battery chargers and grid connection of renewable energy sources.